MDPI

*Article*

# Manifestation of Supramolecular Chirality during Adsorption on CsCuCl₃ and γ-Glycine Crystals

Ilya Zinovyev [1], Ekaterina Ermolaeva [1], Yuliya Sharafutdinova [1], Elmira Gilfanova [1], Leonard Khalilov [2], Irina Pavlova [2] and Vladimir Guskov [1,*]

[1] Department of Chemistry, Ufa University of Science and Technology, 32 Zaki Validi Str., 450076 Ufa, Russia
[2] Ufa Federal Research Centre of the Russian Academy of Sciences (UFRC RAS), Institute of Petrochemistry and Catalysis RAS, 141 Oktyabrya Av., 450075 Ufa, Russia
* Correspondence: guscov@mail.ru

**Abstract:** The chirality of biopolymers and its emergence from the racemic prebiotic world is one of the key mysteries of science. There are many versions on how the total chiral balance breaking occurred, but they all face an insoluble challenge—the impossibility of a total shift of the chiral balance towards the formation of biopolymers based only on D-sugars and L-amino acids. A possible solution to this problem lies in the asymmetric autocatalysis on chiral crystals. Since the reaction is heterogeneous, it is important to study the features of adsorption on the surface of crystals. In this paper, the adsorption of limonene, α-pinene, and menthol enantiomers on γ-glycine and CsCuCl₃ crystals was studied. Single-crystal X-ray crystallography, SEM, and porosimetry were used as auxiliary methods. The *t*-test was used to determine the reliability of chiral recognition. It was shown that both crystals were capable of chiral recognition at high coverages. The mechanism of supramolecular chiral recognition was identical to that of the chiral crystals studied previously. However, neither γ-glycine nor CsCuCl₃ showed chiral recognition with respect to all enantiomers. In fact, γ-glycine crystals showed recognition for limonene enantiomers, and very high recognition in the case of menthol enantiomers. CsCuCl₃ crystals showed the capability to recognize enantiomers of α-pinenes only. This led to the conclusion that the recognition of enantiomers by a supramolecular chiral surface is not universal.

**Keywords:** supramolecular chirality; chiral crystals; enantiomer adsorption; supramolecular chiral surface; Viedma ripening

## 1. Introduction

Chirality is a geometric feature that is observed at all hierarchy levels of matter. In an n-dimensional space, an object or a set of objects is chiral if it cannot be superimposed on its mirror image by movements in that space [1]. Chemical, physical, biological, and even mathematical objects can be chiral. For example, the well-known Möbius strip is a chiral object. In elementary particle physics, chirality is connected to the parity conservation. Therefore, only left-handed helical neutrinos are found [2]. The parity violation has been a well-studied effect since 1956. In fact, it has been shown that the parity principle might be invalid for certain weak interactions, such as those involved in β-decay [3]. In chemistry, chirality is observed as the presence of a center, axis or plane of chirality in chemical molecules. Most often, chiral molecules have an asymmetric carbon atom. Many biological objects, circularly polarized light, and even galaxies are chiral objects [4].

Between chiral molecules and the RNA-world, the supramolecular chirality exists. Supramolecular chirality is the result of the special spatial arrangements of molecules [2,5,6]. All polypeptides, DNA, and RNA are supramolecular chiral structures due to the formation of right-handed α-helixes [7,8]. Any living organism is a complex supramolecular chiral system that consists of many "building blocks". The effect of supramolecular chirality is believed to be a key to the emergence of life [9]. There are as many examples of

supramolecular chirality as of molecular chirality: various 2D crystals [10,11], the surface of chiral 3D crystals [12,13], 2D supramolecular structures [14–18], helices [19–22], hierarchical self-assembly structures [23,24], and enantiotopic surfaces of achiral crystals [25,26]. However, it remains unknown how the conversion from racemic molecular building blocks to homochiral biopolymers occurred [27,28]. Further, while there are enough reasons for chiral symmetry breaking [29–31], there is no solution to the challenge on how a minute shift of chiral symmetry led to complete deracemization.

Asymmetric autocatalysis provides one of the possible ways for understanding the pathways of total deracemization. In asymmetric autocatalysis, each enantiomer catalyses the production of itself, while suppressing that of its mirror image [32,33]. In asymmetric autocatalysis even a minute enantiomer excess (*ee*) leads to complete deracemization. However, only two examples of such a process are known to date: the Soai reaction [34,35] and Viedma ripening [32,36]. In both cases, enantiomorphic crystals are considered. Since these crystals are solids, autocatalysis in the Soai reaction is triggered by a heterogeneous process with adsorption as the first stage. Therefore, it is important to study the process of chiral recognition during adsorption on a crystal surface with supramolecular chirality.

Chiral crystals are usually formed by molecules with an asymmetric carbon atom [37]. However, in some cases, achiral compounds crystallize as chiral crystals [13,38]. A prerequisite for the formation of chiral crystals is that crystallization should occur in one of 65 noncentrosymmetric Sohncke space groups [39]. Those 65 space groups include 11 pairs of enantiomorphous crystal classes. Such space groups are inherently chiral, and when one enantiomer crystallizes in one of such enantiomorphous groups, the opposite enantiomer will crystallize in the opposite space group of the pair [1]. We denote crystals with such space groups as the first type of chiral crystals. In previous works, the adsorption of enantiomers on crystals of nickel sulfate hexahydrate [40], cytosine [41], hippuric acid, and phloroglucinol [42] was studied. It was found that enantiomers recognition by supramolecular chiral surface was observed only at high surface coverages. At such coverages, lateral interactions between adsorbed molecules were observed, and the isotherm deviated from linearity. The surface does not recognize individual molecules, but recognizes an adsorption layer of enantiomers by promoting the formation of a layer of one enantiomer and suppressing the formation of a layer of the other one (Figure 1). However, much remains unclear. In fact, all the crystals studied previously belonged to the second type of chiral crystals that crystallize in an achiral space group but undergo only operation of the first kind. In this case, the asymmetry element is located inside the chiral crystal and consists of several mutually ordered molecules. Both enantiomorphs have the same space symmetry group. The adsorption on chiral crystals of the first type has not been studied to date. Additionally, the universality/selectivity of enantiomer recognition by a supramolecular chiral surface remains unclear. In this work, we have studied the adsorption of enantiomers on two first-type chiral crystals, $CsCuCl_3$, and γ-glycine. γ-Glycine crystallizes as a chiral conglomerate with symmetry group $P3_1$ or $P3_2$ [43]. Chiral γ-glycine crystals were successfully used in asymmetric autocatalysis by the Soai team [44]. For $CsCuCl_3$ there is no information about its application for chiral recognition, but the crystal space group was determined as $P6_122$ and $P6_522$.
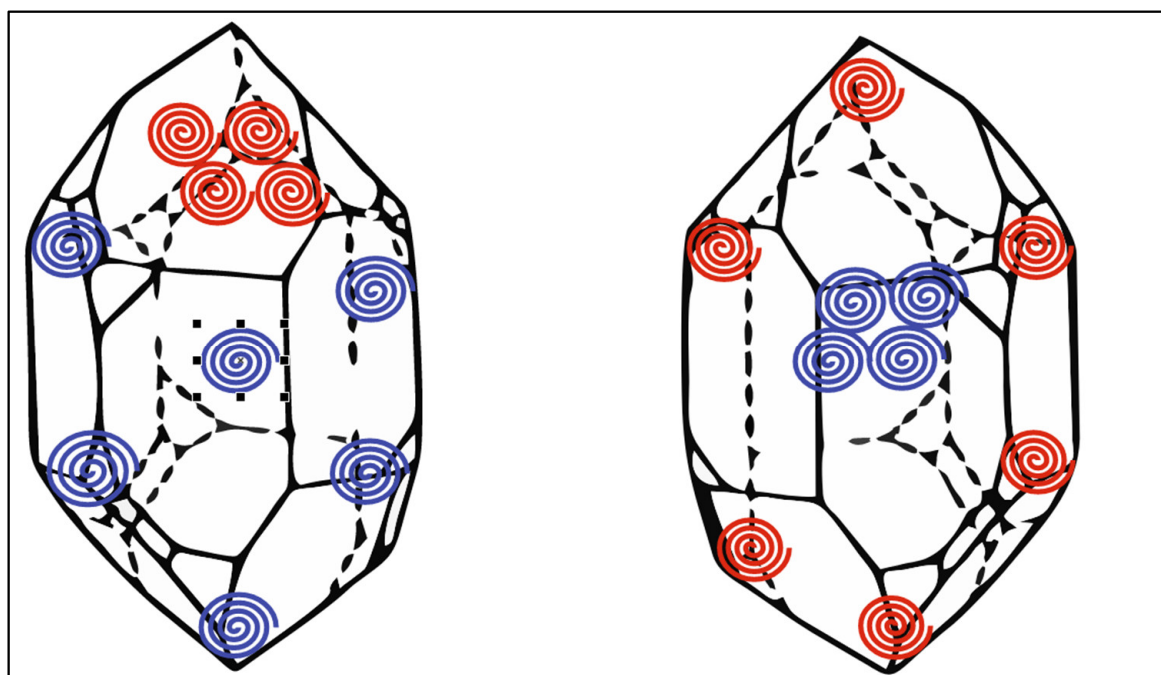
**Figure 1.** The supramolecular chiral recognition by a chiral crystal surface.

## 2. Materials and Methods

### 2.1. Materials

The chiral crystals of γ-glycine were obtained from glycine (>99%, Sigma-Aldrich, Burlington, MA, USA, CAS: 56-40-6) and those of $CsCuCl_3$, from CsCl (>99%, Reakhim, Saint Petersburg, Russia, CAS: 7647-17-8) and $CuCl_2$ (>99%, Reakhim, Saint Petersburg, Russia, CAS: 7447-39-4). Silica gel KSM-5 (Reakhim, Saint Petersburg, Russia, CAS: 112926-00-8) was used as the solid support for the crystals.

Highly purified water with a conductivity less than 10 μS/m obtained using a DV-10UV water deioniser (TsvetChrom, Dzerzhinsk, Russia) and aqueous ammonia (Reakhim, Saint Petersburg, Russia, CAS: 7664-41-7) were used as the solvents for crystallization. To obtain adsorption isotherms from solutions, n-heptane (>99.5%, Ekos-1, Moscow, Russia, CAS 142-82-5) and chloroform (>99%, Ekos-1, Moscow, Russia, CAS 67-66-3) were used as the solvents, while D-menthol (99.9%, Sigma-Aldrich, Burlington, MA, USA, CAS 15356-60-2) and L-menthol (99.4%, SigmaAldrich, Burlington, MA, USA, CAS 2216-51-5) were used as the adsorbing molecules.

In determination of vapor adsorption isotherms, D-limonene (97%, Sigma-Aldrich, Milwaukee, WI, USA, CAS 5969-27-5), L-limonene (96%, Sigma-Aldrich, Milwaukee, WI, USA, CAS 5989-54-8), D-α-pinene (>99%, Sigma-Aldrich, Milwaukee, WI, USA, CAS 7785-70-8), and L-α-pinene (97%, Sigma-Aldrich, Milwaukee, WI, USA, CAS 7785-26-4) were used. Helium (>99.995%, Techgas, Orenburg, Russia, CAS 14762-55-1) was used as the carrier gas in chromatographic experiments.

### 2.2. Methods

#### 2.2.1. γ-Glycine Crystallization under Viedma Ripening Conditions

Glycine (38.18 g), an aqueous solution of ammonia (110 mL), glass beads (10 g), and glycine crystals were placed into a conical flask. The chemicals were stirred at 500 rpm and a temperature of 33 °C. After complete dissolution, the solution was cooled to T = 20 °C, then heated again. After redissolving, the temperature was gradually lowered by 1 °C/15 min. The solution was then left for 2 days. After that time, the precipitate was filtered off and the sorbent was dried in an oven. The procedure was repeated twice.

### 2.2.2. CsCuCl$_3$ Crystallization under Viedma Ripening Conditions

A saturated solution of CsCl (57.2 g) in acidified water was gradually added to a solution of 110.8 g of CuCl$_2$ at 32 °C (pH = 1.39) with continuous stirring. The resulting solution was vigorously stirred with glass beads at a speed of 1300 rpm. The temperature was then reduced to 25 °C and stirring was continued for 2 days. The resulting suspension was left for 7 days in an open flask. The suspension was then filtered off and the resulting precipitate was dried for one day. After that, the precipitate was additionally dried in a stream of nitrogen for one hour. As a result, garnet-black crystals were obtained.

### 2.2.3. Single-Crystal X-ray Crystallography

A suitable crystal was selected on a Xcalibur, Eos diffractometer. The crystal was kept at 293 K during data collection. Using Olex2 [45], the structure was solved with the SHELXT structure solution program using Intrinsic Phasing and refined with the SHELXL [46] refinement package using Least Squares minimisation.

### 2.2.4. Silica Gel Modification

γ-Glycine (4.7 g) was added to a saturated glycine solution, and the solution was then stirred for two hours at room temperature at a speed of 1500 rpm. Silica gel with a fraction size of 0.25–0.3 mm (47 g) was added. Stirring was continued at a speed of 200–300 rpm for a few hours. The sorbent was then filtered off and dried at a temperature of 100 °C.

A saturated solution of CsCl in acidified water was gradually added to a solution of CuCl$_2$ (pH = 1.39) with continuous stirring. Additionally, 5 g of the previously obtained CsCuCl$_3$ crystals was added to the solution which was then stirred for 30 min. Next, 50 g of silica gel was added. The solution was evaporated at room temperature with stirring until the latter was no longer possible.

### 2.2.5. SEM of Modified Silica Gel Samples

Scanning electron microscopy was applied to study the surface morphology of silica gel samples modified with γ-glycine or CsCuCl$_3$, respectively. A Hitachi Regulus SU8220 microscope at a voltage of 1–2 kV and a working distance of 8 mm was used. The samples were applied to a conductive carbon adhesive tape attached to an aluminum SEM sample holder.

### 2.2.6. Porosity Characterization

The analysis was conducted by nitrogen adsorption-desorption at 77 K on a Quantachrome NOVA1200e sorbtomer. Before the analysis, silica gel samples modified with γ-glycine or CsCuCl$_3$ crystals, respectively, were evacuated at 200 °C for 6 h. The specific surface area (S, m$^2$/g) was calculated at a relative partial pressure of P/P$^0$ = 0.3. The mesopore volume (V$_p$, cm$^3$/g) and pore diameter (D$_p$, Å) were determined by the BJH method at a relative partial pressure of P/P$_0$ = 0.95. The presence of micropores was determined by de Boer and Lippens t-graph as reported previously [40].

### 2.2.7. Enantiomer Vapor Adsorption under Gas Chromatography Conditions

The adsorption of limonene and α-pinene vapors on the crystals was studied. The 120–250 μm crystal fraction was placed into a 1000 mm × 3 mm stainless steel column. Enantiomer adsorption was studied by inverse gas chromatography at finite concentration using a Chromos GC-1000 gas chromatograph (Himanalitservice, Dzerzhinsk, Russia) equipped with a flame ionization detector. The column temperature ranged from 80 °C to 160 °C. The temperature of the injector and detector was 200 °C. The flow rate of helium carrier gas varied from 2 to 5 mL/min. The enantiomers were injected as liquids with a volume ranging from 2 μL to 7 μL. Here and in Section 2.2.8, at least 5 parallel experiments were performed.

2.2.8. Adsorption of Menthols from Solutions

A 0.5 g sample of silica gel modified with $CsCuCl_3$ was introduced into D- and L-menthol solutions in n-heptane. The solution volume was 30 mL, and the menthol concentration ranged from 25 µg/mL to 300 µg/mL. The solution with the adsorbent was shaken for 1 h at 25 °C.

Silica gel modified with γ-glycine clumps in n-heptane, so chloroform was used as the solvent. The concentrations of menthol enantiomers varied from 100 to 600 µg/mL. The other experimental conditions were identical to those with $CsCuCl_3$.

The variation of menthols' concentration in solutions was monitored by gas chromatography. The measurement conditions were identical to those described previously [40,42].

*2.3. Calculations*

The number of adsorbed molecules and vapor partial pressure were calculated according to the classical Kiselev and Yashin approach [47]. The experimental adsorption isotherms were approximated by the classical Langmuir, Freindlich, and BET equations (according to the isotherm type). To estimate the energy of lateral interactions, the isotherms were additionally fitted by the Fowler–Guggenheim equation [48]:

$$ln\left[\frac{p(1-\theta)}{\theta}\right] = -lnK_{FG} + \frac{2b_f\theta}{RT} \tag{1}$$

where $K_{FG}$ is the Fowler–Guggenheim constant and $b_f$ is the lateral interaction energy.

The selectivity factor α was calculated as a ratio (larger to smaller) of enantiomer adsorption values at the same concentration (pressure).

To establish the difference in adsorption values, a Student's *t*-test was used. This statistical method involves testing a null hypothesis about the coincidence of two sets of adsorption data (for each of the enantiomers) by calculating the experimental values of the *t*-test and the corresponding *p*-value, and comparing the latter value with the pre-chosen significance levels α [49]. If the *p*-value was smaller than the significance level, the alternative hypothesis was true—the enantiomer adsorption values are different. The adsorption isotherms approximation parameters, as well as all the points on the different adsorption isotherms, were processed using the *t*-test.

**3. Results**

*3.1. Properties of γ-Glycine and $CsCuCl_3$ Crystals and Silica Gel-Based Adsorbents*

Single-crystal X-ray crystallography was used to confirm the required structure and symmetry space group of the crystals obtained. The structure data of the crystals studied are presented in Table 1. As follows from the data obtained, the crystal lattice parameters for the crystallization products described in Section 2.2.1 corresponded to γ-glycine [50] and $CsCuCl_3$ [51]. Since the enantiomorphs of both crystals studied have different space symmetry groups, the X-ray diffraction data confirmed that the crystallized γ-glycine and $CsCuCl_3$ belonged to only one type of enantiomorphs.

Figure 2 shows the SEM images of silica gel samples modified with γ-glycine and $CsCuCl_3$. As one can see from the figure, in both cases, impregnated modifier crystals can be discerned on the silica gel surface. There is no complete surface coverage, as the crystals are solids, however full coverage is not required. Silica gel is only a carrier of small crystals, and makes it possible to increase the specific surface area of the crystals. The latter is critical for the study of adsorption processes, since a low specific surface area usually makes it difficult to reliably measure the amount of adsorbed molecules on nonporous solids. Data of the specific surface area and other surface and porosity characteristics of the studied samples are given in Table 2.

The porosity characteristics of silica gel samples modified with various crystals differ dramatically. In fact, the specific surface area differs more than 3-fold, while silica gel modified with $CsCuCl_3$ has no micropores. The average pore size also differs almost 3-fold.

The results obtained indicate the difference in γ-glycine and $CsCuCl_3$ crystallization on the silica gel surface. Probably, the latter compound can crystallize in the pores of silica gel, while glycine preferentially crystallizes on the surface of a silica gel particle, almost without filling the micropores. It can be explained by the strong H-bonding between the glycine molecules and the silica gel surface.

**Table 1.** Crystallographic data of the crystals studied.

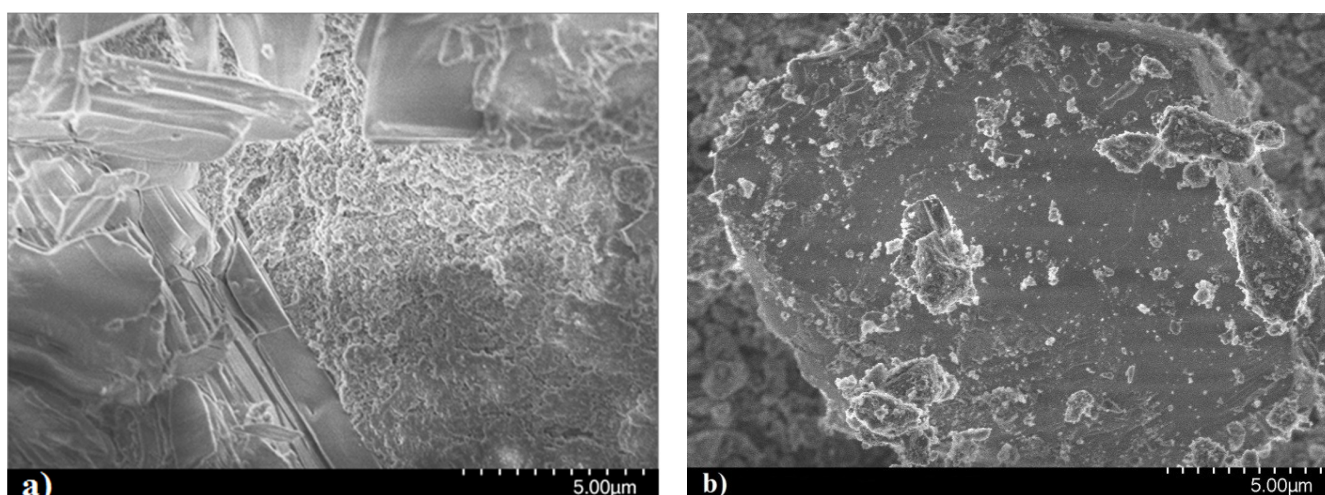|  | γ-Glycine | $CsCuCl_3$ |
|---|---|---|
| Empirical formula | $C_2H_5NO_2$ | $Cl_3CsCu$ |
| Formula weight | 75.07 | 302.80 |
| Crystal system | trigonal | hexagonal |
| Space group | $P3_2$ | $P6_122$ |
| a, Å | 7.0390(2) | 7.1979(5) |
| b, Å | 7.0390(2) | 7.1979(5) |
| c, Å | 5.4794(2) | 18.1525(13) |
| α, ° | 90 | 90 |
| β, ° | 90 | 90 |
| γ, ° | 120 | 120 |
| Volume, Å$^3$ | 235.118(16) | 814.48(13) |
| Z | 3 | 6 |
| $\rho_{calc}$, g/cm$^3$ | 1.591 | 3.704 |
| μ, mm$^{-1}$ | 0.141 | 11.930 |
| F(000) | 120.0 | 810 |
| Radiation | MoKα (λ = 0.71073) | MoKα (λ = 0.71073) |
| 2Θ range, ° | 6.684 to 57.902 | 6.536 to 64.216 |
| Index ranges | $-8 \leq h \leq 9, -9 \leq k \leq 8, -6 \leq l \leq 6$ | $-9 \leq h \leq 9, -8 \leq k \leq 8, -25 \leq l \leq 15$ |
| Reflections collected | 3336 | 3046 |
| Independent reflections | 765 [$R_{int}$ = 0.0277, $R_{sigma}$ = 0.0161] | 872 [$R_{int}$ = 0.0831] |
| Goodness-of-fit on F$^2$ | 1.120 | 1.044 |
| Final R indexes [I $\geq$ 2σ (I)] | $R_1$ = 0.0224, $wR_2$ = 0.0581 | $R_1$ = 0.0566, $wR_2$ = 0.1219 |
| Final R indexes [all data] | $R_1$ = 0.0227, $wR_2$ = 0.0585 | $R_1$ = 0.0724, $wR_2$ = 0.1343 |
| Largest diff. peak/hole/e Å$^{-3}$ | 0.20/−0.12 | 1.19/−2.94 |
| Flack parameter | −0.6(4) | −0.02(8) |



**Figure 2.** SEM images of silica gel modified by (**a**) γ-glycine; (**b**) $CsCuCl_3$.

**Table 2.** Total specific surface area $S$ (m$^2$/g), specific surface area of micropores $S_m$ (m$^2$/g), total pore volume $V$ (mL/g), micropore volume $V_m$ (mL/g), and average pore diameter $D_p$ (Å) of silica gel samples modified by $\gamma$-glycine and CsCuCl$_3$.

| Silica Gel | Initial | +$\gamma$-Glycine | +CsCuCl$_3$ |
|:---:|:---:|:---:|:---:|
| $S$ | 350 | 690 | 166 |
| $S_m$ | 0 | 220 | 0 |
| $V$ | 0.83 | 1.02 | 0.42 |
| $V_m$ | 0 | 0.12 | 0 |
| $D_p$ | 41 | 15 | 41 |

*3.2. Isotherms of Enantiomer Vapors on the Crystals Studied*

Figure 3 shows some vapor isotherms of limonene enantiomers on $\gamma$-glycine crystals. The isotherms at other temperatures are given in Supplementary Materials. The isotherms of limonenes at 90 °C do not coincide visually (Figure 3a). However, statistical analysis of the differences in adsorption values using the *t*-test has shown no significant differences in the adsorption of limonenes at any coverages (Table 3).
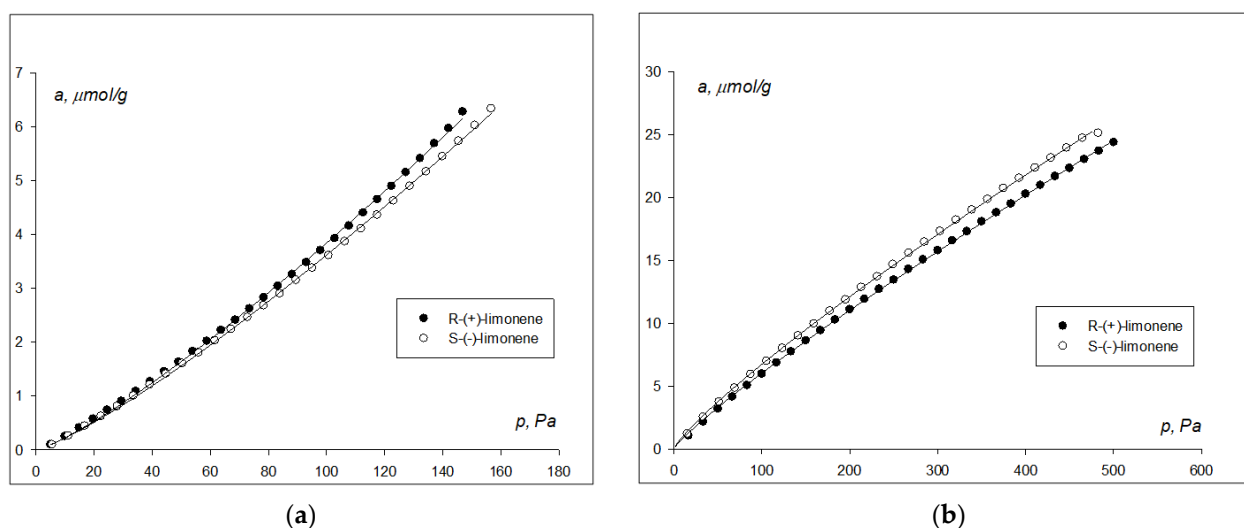


(**a**)



(**b**)

**Figure 3.** Adsorption isotherms of limonene vapors on $\gamma$-glycine crystals at (**a**) 90 °C; (**b**) 150 °C.

**Table 3.** *p*-values for pairs of points of limonenes adsorption isotherms on $\gamma$-glycine crystals at 90 °C ($\alpha$ = 0.05).

| P, Pa | *p* | P, Pa | *p* | P, Pa | *p* |
|:---:|:---:|:---:|:---:|:---:|:---:|
| 0.7 | 0.2501 | 10.8 | 0.3659 | 16.6 | 0.0756 |
| 1.4 | 0.0199 | 11.5 | 0.4172 | 17.4 | 0.3346 |
| 7.3 | 0.1103 | 12.3 | 0.2163 | 18.1 | 0.4641 |
| 8.0 | 0.2362 | 13.0 | 0.1752 | 18.8 | 0.5849 |
| 8.8 | 0.8444 | 13.9 | 0.1013 | 19.5 | 0.6044 |
| 9.5 | 0.8052 | 14.5 | 0.0839 | 20.3 | 0.7399 |
| 10.1 | 0.5798 | 15.4 | 0.0820 | 21.0 | 0.7459 |

Thus, the values of limonene enantiomers' adsorption on $\gamma$-glycine crystals were the same in all parts of the adsorption isotherm. The lack of ability to recognize enantiomers was observed in the temperature range of 90–120 °C (the other isotherms are provided

in Supplementary Materials). Further, at those temperatures, the shape of all adsorption isotherms corresponds to BET type III. Therefore, in the "achiral region" of temperatures, interactions between limonenes on the $\gamma$-glycine surface are stronger than the limonene-glycine interactions.

At the same time, at 150 °C, a visual difference in adsorption isotherms was also observed (Figure 3b). However, *t*-test has shown a significant difference in adsorption values even at a pressure of 1.37 kPa (the third point on the isotherm, see Table 4). At all higher pressures, a difference in adsorption values was also observed. Therefore, at a temperature of 150 °C, the adsorption of limonene enantiomers was different at the majority of coverages. The absence of differences in the initial region of the isotherm (in the Henry region) is caused by the lack of lateral interactions between adsorbed molecules. This phenomenon was observed for all the crystals studied previously and was explained in detail in [40].

**Table 4.** *p*-values for pairs of points of limonenes' adsorption isotherms on $\gamma$-glycine crystals at 150 °C ($\alpha$ = 0.05).

| P, kPa | *p* | P, kPa | *p* | P, kPa | *p* |
|--------|------|--------|--------|--------|--------|
| 1.03 | 0.4259 | 2.39 | 0.0032 | 3.41 | 0.0039 |
| 1.19 | 0.0589 | 2.56 | 0.0072 | 3.59 | 0.0039 |
| 1.37 | 0.014 | 2.73 | 0.0224 | 3.76 | 0.0044 |
| 1.54 | 0.0177 | 2.90 | 0.0345 | 3.93 | 0.0002 |
| 1.71 | 0.0301 | 3.07 | 0.0009 | 4.10 | 0.0002 |
| 2.22 | 0.0012 | 3.24 | 0.0012 | 4.27 | 0.0002 |

Thus, in analyzing adsorption isotherms, it is not enough to identify a difference in adsorption values visually, even if it seems significant. The conclusion about the difference in adsorption isotherms can only be made by statistical analysis.

A noticeable difference in the adsorption isotherms of limonenes on $\gamma$-glycine was observed in the temperature range of 130–150 °C. In all cases, S-(−)-limonene was adsorbed more strongly than R-(+)-limonene. No differences were found at 160 °C. The isotherm shapes at these temperatures differ from those at 90–120 °C. In fact, the isotherm at 130 °C is nearly linear, while the isotherms at 140–150 °C can be classified as BET type I. Hence, in the "chiral region" of temperatures, the interactions between adsorbed limonene molecules are close to (130 °C) or weaker than (140 and 150 °C) limonene-glycine interactions.

A different dependence was observed in the case of limonenes' adsorption on $CsCuCl_3$ crystals. In this case, no significant differences in adsorption isotherms were found at all temperatures (Figure 4). The lack of any differences was also confirmed by the *t*-test data (Tables S16–S20 in Supplementary Materials). Thus, the adsorption of limonenes on $\gamma$-glycine and $CsCuCl_3$ crystals differs dramatically.

In addition to limonenes, the adsorption of $\alpha$-pinene enantiomers was studied. The difference between these non-polar compounds and limonenes lies in the more bulky structure of the cycle. As a result, it is more difficult to obtain a stable layer of pinenes on a flat surface. Moreover, fewer carbon atoms are able to interact with the surface in the adsorbed state. The adsorption isotherms of these compounds on the crystals studied are shown in Figure 5.

It is noticeable that the chiral recognition by $CsCuCl_3$ crystals with respect to $\alpha$-pinenes turned out to be higher than with respect to limonenes. In fact, the adsorption of (+)-$\alpha$-pinene was noticeably higher than that of (−)-$\alpha$-pinene at all temperatures below 150 °C. In this case, like in the case of limonenes, the isotherms of $\alpha$-pinenes are nearly linear.
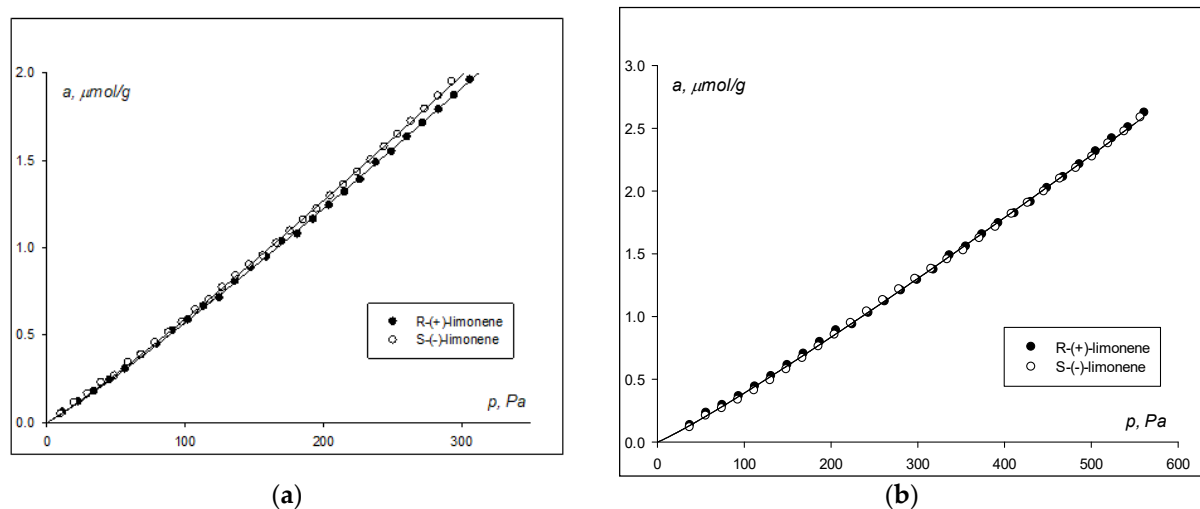
**(a)**

**(b)**

**Figure 4.** Isotherms of limonene vapors' adsorption by CsCuCl$_3$ crystals (**a**) at 100 °C; (**b**) at 120 °C.



**(a)**

**(b)**
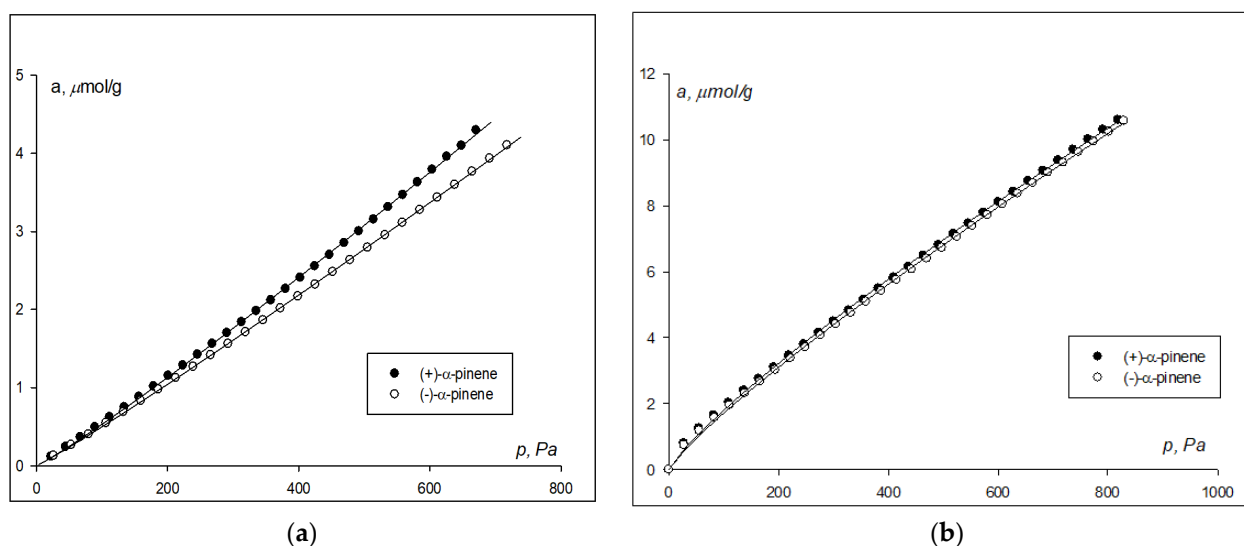
**Figure 5.** Isotherms of $\alpha$-pinenes vapors' adsorption (**a**) by CsCuCl$_3$ crystals at 100 °C; (**b**) by $\gamma$-glycine crystals at 90 °C.

This phenomenon is unusual, since in previous studies, the selectivity of chiral crystals for $\alpha$-pinenes was usually lower than for limonenes. In the case of $\gamma$-glycine, the recognition with respect to $\alpha$-pinenes is also weaker than with respect to limonenes (Figure 5b), because the adsorption values of $\alpha$-pinenes do not differ at any temperature. The lower selectivity of the surface of enantiomorphic crystals to $\alpha$-pinenes is caused by the molecule structure, which prevents strong lateral interactions and the formation of a dense enantiomer layer.

Approximation of the adsorption isotherms by the Freundlich, Langmuir, and Fowler–Guggenheim equations confirms the above conclusions. In fact, the Langmuir constants $K_L$ at 140 and 150 °C for S-($-$)-limonene on $\gamma$-glycine are higher than for R-(+)-limonene (Table 5). The Fowler–Guggenheim constants change in a similar way. The energy of lateral interactions $b_f$ differs significantly at the same temperatures. Since for the same ordering degree of the adsorption layer, $b_f$ is always the same for enantiomers, the difference in the energy of lateral interactions is caused by the different structure of the enantiomer layer on the surface. The latter occurs as a result of chiral recognition by the crystal surface. It is possible that the enantiomer layer on the surface with supramolecular chirality forms something like a chiral 2D crystal/2D supramolecular structure, similarly to the processes of self-assembly of nonpolar or weakly polar compounds described in the literature [4,10,52].

Chiral molecules always form a 2D crystal with a chiral wallpaper group [10], so the resulting enantiomer layer should be supramolecular chiral.

**Table 5.** The results of approximation of limonenes' adsorption isotherms on γ-glycine crystals by Langmuir and Fowler–Guggenheim equations ($K_L$—Langmuir constant, $K_{FG}$—Fowler–Guggenheim constant, $a_m$—monolayer capacity, μmol/g, $b_f$—lateral interaction energy, kJ/mol).

| T, °C | $K_L \times 10^3$ | | $a_m$ | | $K_{FG} \times 10^3$ | | $b_f$ | |
|---|---|---|---|---|---|---|---|---|
| | R-(+) | S-(−) | R-(+) | S-(−) | R-(+) | S-(−) | R-(+) | S-(−) |
| 140 | $5.0 \pm 0.2$ | $6.0 \pm 0.2$ | $149 \pm 5$ | $129 \pm 3$ | 4.6 | 5.8 | 0 | 0.08 |
| 150 | $6.0 \pm 0.3$ | $9.0 \pm 0.3$ | $104 \pm 3$ | $79 \pm 5$ | 5.9 | 8.8 | 0.09 | 0.28 |
| 160 | $4.0 \pm 0.2$ | $4.0 \pm 0.2$ | $193 \pm 2$ | $177 \pm 2$ | 3.5 | 4.0 | 0.09 | 0.11 |

### 3.3. Isotherms of Menthols' Adsorption from Solutions

The differences in the manifestation of chiral recognition between γ-glycine and $CsCuCl_3$ crystals were more noticeable in the case of the adsorption of menthols from solutions at 25 °C (Figures 6 and 7). In fact, the adsorption isotherms coincided on a silica gel sample modified with $CsCuCl_3$ until a monolayer (a ≈ 45 μmol/g) was attained. Only above a monolayer, some difference in adsorption values was observed, which disappeared at θ = 1.5. The isotherms could be classified as similar to BET type II.
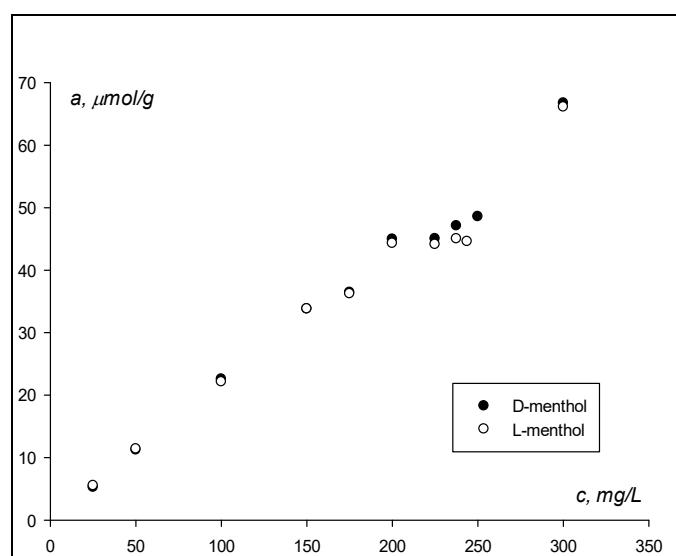


**Figure 6.** Adsorption isotherm of menthols on silica gel modified with $CsCuCl_3$.

The isotherms on glycine differed almost at all concentrations. Moreover, the shape of the isotherms for the enantiomers differed. In the case of D-menthol, at all concentrations except 600 mg/L, the adsorption values remained unchanged at the level of 3–6 μmol/g. For L-menthol, the adsorption values increased to reach a monolayer at a = 40 μmol/g (similarly to $CsCuCl_3$). At higher concentrations, the formation of a second layer of menthol began.

It is unusual that the adsorption values differ significantly between the enantiomers. The monolayer capacity differed by a factor of 10. Compared to D-menthol, L-menthol was almost not adsorbed on glycine.

The high recognition of γ-glycine crystals with respect to menthol enantiomers made it possible to create a method for the semi-preparative isolation of pure enantiomers. A glass column 50 cm long was filled with γ-glycine-modified silica gel with a fraction of 0.25–0.5 mm. Next, a sample of menthol racemate with a concentration of 350 mg/L was

injected. Chloroform was passed through the column using a perylstatic pump. Samples of the eluate (4 mL) were taken at the column outlet and analyzed with an Atago AP-300 polarimeter (Atago, Japan). It was found that the angle of rotation of plane-polarized light was negative for eluate samples from 8 to 24 mL, while for samples from 44 to 60 mL it was positive. Hence, a semi-preparative separation of the menthols occurred.
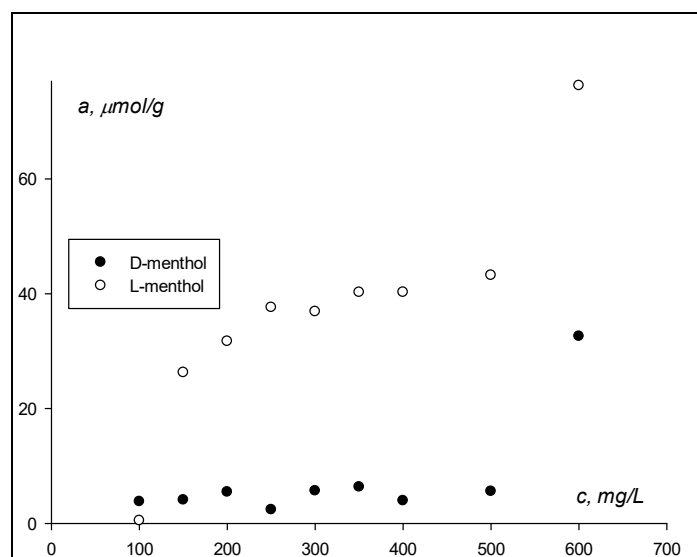


**Figure 7.** Adsorption isotherm of menthols on silica gel modified with γ-glycine.

## 4. Discussion

The observed regularities in the adsorption of limonenes can be explained by the shape of the observed adsorption isotherms. In fact, almost linear adsorption isotherms were observed on $CsCuCl_3$. Probably, since the surface of the crystals is ionized, non-polar limonenes cannot be adsorbed close enough to each other to begin layer formation. Since the layer is not formed, the limonene enantiomer recognition by the surface is impossibile. The ability to form an enantiomer layer on a supramolecular chiral surface is a key point in the supramolecular chiral recognition. Chirality is a geometric phenomenon, and recognition of a chiral object is possible only by a similar chiral object. An achiral object cannot recognize a chiral one under any circumstances. However, if the chirality hierarchy levels do not match, then the objects appear achiral to each other. Therefore, the molecules cannot recognize the difference in chirality of subatomic particles, and the objects with supramolecular chirality cannot recognize structures where the chirality is at molecular hierarchy level.

In order to enable a supramolecular chiral surface "respond" to adsorbed substances, the chirality element dimension of the latter must be comparable to the dimension of the surface chirality element. This becomes possible when the molecules form an adsorption layer on the surface. If such a layer cannot form, no chiral separation is be observed.

In the case of adsorption of limonenes on γ-glycine, the emergence of chiral recognition with increasing temperature can also be explained by the shape of the adsorption isotherm. In the temperature range of 90–120 °C, the predominant lateral interactions of limonene molecules on the glycine surface can lead to the formation of a second adsorption layer before the formation of the first one is completed. When the second layer is formed, the heat of adsorption is equal to the heat of condensation, which is the same for enantiomers. As a result, recognition of enantiomers ceases [41]. Therefore, in the case of type III isotherms, it is always more difficult to find chiral discrimination than in the case of other types of isotherms. The variation in the shape of adsorption isotherm at temperatures above 120 °C was probably caused by the following: with an increase of temperature, the energy of lateral interactions in comparison with the "adsorbed substance—adsorbent" interactions decreased more significantly.

The high chiral recognition of $\gamma$-glycine crystals with respect to menthols can be explained by the formation of a hydrogen bond between a menthol and the $\gamma$-glycine surface. The molecule of the latter has lone electron pairs on the nitrogen atom and two oxygen atoms, which are capable of donor-acceptor interactions with the hydrogen of the menthol hydroxyl group. Further, the hydrogen of the carboxyl group can form donor-acceptor bonds with the lone electron pairs of oxygen in the hydroxyl group of menthol. As a result, one glycine molecule is capable of forming hydrogen bonds with up to 4 menthol molecules. Since hydrogen bonds are stronger than van der Waals interactions, menthol should only interact with the surface with the hydroxyl group. As a result, a dense layer of menthol molecules can be formed on the surface of glycine.

At the same time, in a $CsCuCl_3$ crystal, only chlorine is capable of donating lone electron pairs, while the affinity of the chloride ion to be an electron pair donor is low due to its completed electron shell. Thus, the donor-acceptor interactions between the $CsCuCl_3$ surface and menthol molecules are noticeably weaker than in the case of $\gamma$-glycine. This explains the difference in chiral recognition.

### 5. Conclusions

It was found in this paper that chiral crystals of both $\gamma$-glycine and $CsCuCl_3$ were capable of chiral recognition during adsorption. $\gamma$-Glycine showed recognition with respect to limonene enantiomers and very high recognition with respect to menthol enantiomers. This has made it possible to create the first semi-preparative chromatographic column for the isolation of menthol enantiomers. Crystals of $\gamma$-glycine showed no selectivity with respect to $\alpha$-pinene enantiomers. $CsCuCl_3$ crystals showed a noticeable recognition with respect to the latter. Thus, this work has shown that the chiral recognition of a supramolecular chiral surface is not universal.

## References

1. Viedma, C.; Coquerel, G.; Cintas, P. Crystallization of Chiral Molecules. In *Handbook of Crystal Growth*; Elsevier: Amsterdam, The Netherlands, 2015; pp. 952–1002.
2. Liu, M.; Zhang, L.; Wang, T. Supramolecular chirality in self-assembled systems. *Chem. Rev.* **2015**, *115*, 7304–7397. [CrossRef]
3. Bonner, W.A. *Origins of Chiral Homogeneity in Nature*; John Wiley&Sons, Inc.: Hoboken, NJ, USA, 1988; Volume 18, p. 96.
4. Dutta, S.; Gellman, A.J. Enantiomer surface chemistry: Conglomerate versus racemate formation on surfaces. *Chem. Soc. Rev.* **2017**, *46*, 7787–7839. [CrossRef]
5. Mateos-Timoneda, M.A.; Crego-Calama, M.; Reinhoudt, D.N. Supramolecular chirality of self-assembled systems in solution. *Chem. Soc. Rev.* **2004**, *33*, 363–372. [CrossRef]
6. Borovkov, V. Supramolecular chirality in porphyrin chemistry. *Symmetry* **2014**, *6*, 256–294. [CrossRef]
7. Blackmond, D.G. The Origin of Biological Homochirality. *Cold Spring Harb. Perspect. Biol.* **2019**, *11*, a032540. [CrossRef]

8.   Yang, Y.; Zhang, Y.; Wei, Z. Supramolecular helices: Chirality transfer from conjugated molecules to structures. *Adv. Mater.* **2013**, *25*, 6039–6049. [CrossRef]

9.   Percec, V.; Leowanawat, P. Why are biological systems homochiral. *Isr. J. Chem.* **2011**, *51*, 1107. [CrossRef]

10.  Plass, K.E.; Grzesiak, A.L.; Matzger, A.J. Molecular packing and symmetry of two-dimensional crystals. *Acc. Chem. Res.* **2007**, *40*, 287–293. [CrossRef]

11.  Pakalidou, N.; Mu, J.; Masters, A.J.; Avendano, C. Engineering porous two-dimensional lattices via self-assembly of non-convex hexagonal platelets. *Mol. Syst. Des. Eng.* **2020**, *5*, 376–384. [CrossRef]

12.  Green, B.S.; Lahav, M. Crystallization and solid-state reaction as a route to asymmetric synthesis from achiral starting materials. *J. Mol. Evol.* **1975**, *6*, 99–115. [CrossRef]

13.  Matsumoto, A.; Kaimori, Y.; Kawasaki, T.; Soai, K. Asymmetric autocatalysis initiated by crystal chirality of achiral compounds. In *Advances in Asymmetric Autocatalysis and Related Topics*; Pályi, G., Zucchi, C., Eds.; Elsevier: Amsterdam, The Netherlands, 2017; pp. 337–355.

14.  Gus'kov, V.Y.; Gainullina, Y.Y.; Suhareva, D.A.; Sidel'nikov, A.V.; Kudasheva, F.K. Chiral surfaces formed by uracil, 5-hydroxy-6-methyluracil and melamine supramolecular structures. *Int. J. Appl. Chem.* **2016**, *12*, 359–373.

15.  Zhang, H.-M.; Pei, Z.-K.; Xie, Z.-X.; Long, L.-S.; Mao, B.-W.; Xu, X.; Zheng, L.-S. Preparing self-assembled monolayers of cyanuric acid and melamine complex on HOPG surfaces. *J. Phys. Chem. C* **2009**, *113*, 13940–13946. [CrossRef]

16.  Zhang, H.-M.; Xie, Z.-X.; Long, L.-S.; Zhong, H.-P.; Zhao, W.; Mao, B.-W.; Xu, X.; Zheng, L.-S. One-step preparation of large-scale self-assembled monolayers of cyanuric acid and melamine supramolecular species on Au(111) surfaces. *J. Phys. Chem. C* **2008**, *112*, 4209–4218. [CrossRef]

17.  D'Urso, A.; Marino, N.; Gaeta, M.; Rizzo, M.S.; Cristaldi, D.A.; Fragalà, M.E.; Pappalardo, S.; Gattuso, G.; Notti, A.; Parisi, M.F.; et al. Porphyrin stacks as an efficient molecular glue to induce chirality in hetero-component calixarene–porphyrin assemblies. *New J. Chem.* **2017**, *41*, 8078–8083. [CrossRef]

18.  Nardis, S.; Pomarico, G.; Tortora, L.; Capuano, R.; D'Amico, A.; Natale, C.D.; Paolesse, R. Sensing mechanisms of supramolecular porphyrin aggregates: A teamwork task for the detection of gaseous analytes. *J. Mater. Chem.* **2011**, *21*, 18638–18644. [CrossRef]

19.  Kniazeva, M.V.; Ovsyannikov, A.S.; Samigullina, A.I.; Islamov, D.R.; Gubaidullin, A.T.; Dorovatovskii, P.V.; Lazarenko, V.A.; Solovieva, S.E.; Antipin, I.S.; Ferlay, S. Impact of flexible succinate connectors on the formation of tetrasulfonylcalix[4]arene based nano-sized polynuclear cages: Structural diversity and induced chirality study. *CrystEngComm* **2022**, *24*, 628–638. [CrossRef]

20.  Song, X.; Li, Y.; Gan, L.; Wang, Z.; Yu, J.; Xu, R. Heteroatom-stabilized chiral framework of aluminophosphate molecular sieves. *Angew. Chem. Int. Ed.* **2009**, *48*, 314–317. [CrossRef]

21.  Lin, Z.-E.; Yao, Y.-W.; Zhang, J.; Yang, G.-Y. Synthesis and structure of a novel open-framework zincophosphate with intersecting three-dimensional helical channels. *J. Chem. Soc. Dalton Trans.* **2002**, *24*, 4527–4528. [CrossRef]

22.  Yashima, E.; Maeda, K.; Nishimura, T. Detection and amplification of chirality by helical polymers. *Chem. Eur. J.* **2004**, *10*, 42–51. [CrossRef]

23.  Gaeta, M.; Sortino, G.; Randazzo, R.; Pisagatti, I.; Notti, A.; Fragalà, M.E.; Parisi, M.F.; D'Urso, A.; Purrello, R. Long-range chiral induction by a fully noncovalent approach in supramolecular porphyrin–calixarene assemblies. *Chem. Eur. J.* **2020**, *26*, 3515–3518. [CrossRef]

24.  Nicosia, A.; Vento, F.; Marletta, G.; Messina, G.M.L.; Satriano, C.; Villari, V.; Micali, N.; Martino, M.T.D.; Schotman, M.J.G.; Mineo, P.G. Porphyrin-based supramolecular flags in the thermal gradients' wind: What breaks the symmetry, how and why. *Nanomaterials* **2021**, *11*, 1673. [CrossRef]

25.  Weissbuch, I.; Leiserowitz, L.; Lahav, M. Achiral organic, inorganic, and metal crystals as auxiliaries for asymmetric transformations. *Isr. J. Chem.* **2011**, *51*, 1017–1033. [CrossRef]

26.  Weissbuch, I.; Addad, L.; Leiserowitz, L.; Lahav, M. Total asymmetric transformations at interfaces with centrosymmetric crystals: Role of hydrophobic and kinetic effects in the crystallization of the system glycine/αamino acids. *J. Am. Chem. Soc.* **1988**, *110*, 561–567. [CrossRef]

27.  Davankov, V.A. Biological Homochirality on the Earth, or in the Universe? A Selective Review. *Symmetry* **2018**, *10*, 749. [CrossRef]

28.  Davankov, V.A. Chance and necessity in the evolution of matter to Life: A comprehensive hypothesis. *Symmetry* **2021**, *13*, 1918. [CrossRef]

29.  Korenic, A.; Perovic, S.; Cirkovic, M.M.; Miquel, P.-A. Symmetry breaking and functional incompleteness in biological systems. *Prog. Biophys. Mol. Biol.* **2020**, *150*, 1–12. [CrossRef]

30.  Takahashi, J.-I.; Kobayashi, K. Origin of terrestrial bioorganic homochirality and symmetry breaking in the universe. *Symmetry* **2019**, *11*, 919. [CrossRef]

31.  Arlegui, A.; Soler, B.; Galindo, A.; Arteaga, O.; Canillas, A.; Ribó, J.M.; El-Hachemi, Z.; Crusats, J.; Moyano, A. Spontaneous mirror-symmetry breaking coupled to top-bottom chirality transfer: From porphyrin self-assembly to scalemic Diels–Alder adducts. *Chem. Commun.* **2019**, *55*, 12219–12222. [CrossRef]

32.  Viedma, C. Chiral symmetry breaking during crystallization: Complete chiral purity induced by nonlinear autocatalysis and recycling. *Phys. Rev. Lett.* **2005**, *94*, 065504. [CrossRef]

33.  Frank, F.C. Spontaneous asymmetric synthesis. *Biochim. Biophys. Acta* **1953**, *11*, 459–463. [CrossRef]

34.  Soai, K.; Shibata, T.; Morioka, H.; Choji, K. Asymmetric autocatalysis and amplification of enantiomeric excess of a chiral molecule. *Nature* **1995**, *378*, 767–768. [CrossRef]

35. Soai, K. Asymmetric autocatalysis. Chiral symmetry breaking and the origins of homochirality of organic molecules. *Proc. Jpn. Acad. Ser. B* **2019**, *95*, 89–110. [CrossRef]

36. Sogutoglu, L.-C.; Steendam, R.R.E.; Meekes, H.; Vlieg, E.; Rutjes, F.P.J.T. Viedma ripening: A reliable crystallisation method to reach single chirality. *Chem. Soc. Rev.* **2015**, *44*, 6723–6732. [CrossRef]

37. Walsh, M.P.; Barclay, J.A.; Begg, C.S.; Xuan, J.; Johnson, N.T.; Cole, J.C.; Kitching, M.O. Identifying a hidden conglomerate chiral pool in the CSD. *JACS Au* **2022**, *2*, 2235–2250. [CrossRef]

38. Matsuura, T.; Koshima, H. Introduction to chiral crystallization of achiral organic compounds. Spontaneous generation of chirality. *J. Photochem. Photobiol. C Photochem. Rev.* **2005**, *6*, 7–24. [CrossRef]

39. Sivakumar, R.; Kwiatoszynski, J.; Fouret, A.; Nguyen, T.P.T.; Ramrup, P.; Cheung, P.S.M.; Cintas, P.; Viedma, C.; Cuccia, L.A. Enantiomer-specific oriented attachment of guanidine carbonate crystals. *Cryst. Growth Des.* **2016**, *16*, 3573–3576. [CrossRef]

40. Gus'kov, V.Y.; Allayarova, D.A.; Garipova, G.Z.; Pavlova, I.N. Supramolecular chiral surface of nickel sulfate hexahydrate crystals and its ability to chiral recognition by enantiomers adsorption data. *New J. Chem.* **2020**, *44*, 17769–17779. [CrossRef]

41. Gus'kov, V.Y.; Shayakhmetova, R.K.; Allayarova, D.A.; Sharafutdinova, Y.F.; Gilfanova, E.L.; N.Pavlova, I.; Garipova, G.Z. Mechanism of chiral recognition by enantiomorphous cytosine crystals during enantiomer adsorption. *Phys. Chem. Chem. Phys.* **2021**, *23*, 11968–11979. [CrossRef]

42. Gus'kov, V.Y.; Gallyamova, G.A.; Sairanova, N.A.; Sharafutdinova, Y.F.; Khalilov, L.M.; Mukhametzyanov, T.A.; Zinoviev, I.M.; Gainullina, Y.Y. Possibility of chiral recognition by adsorption on enantiomorphous crystals: The impact of crystal surface polarity. *Phys. Chem. Chem. Phys.* **2022**, *24*, 26785–26794. [CrossRef]

43. Tarasevych, A.V.; Sorochinsky, A.E.; Kukhar, V.P.; Toupet, L.; Crassous, J.; Guillemin, J.-C. Attrition-induced spontaneous chiral amplification of the γ polymorphic modification of glycine. *CrystEngComm* **2015**, *17*, 1513–1517. [CrossRef]

44. Matsumoto, A.; Ozaki, H.; Tsuchiya, S.; Asahi, T.; Lahav, M.; Kawasaki, T.; Soai, K. Achiral amino acid glycine acts as an origin of homochirality in asymmetric autocatalysis. *Org. Biomol. Chem.* **2019**, *17*, 4200–4203. [CrossRef] [PubMed]

45. Dolomanov, O.V.; Bourhis, L.J.; Gildea, R.J.; Howard, J.A.K. OLEX2: A Complete Structure Solution, Refinement and Analysis Program. *J. Appl. Cryst.* **2009**, *42*, 339–341. [CrossRef]

46. Sheldrick, G.M. Crystal structure refinement with SHELXL. *Acta Crystallogr. Sect. C Struct. Chem.* **2015**, *71*, 3–8. [CrossRef] [PubMed]

47. Kiselev, A.V.; Yashin, Y.I. *Gas Adsorption Chromatography*; Plenum Press: New York, NY, USA, 1969.

48. Cerefolini, G.F.; Rudzinski, W. Theoretical principles of single- and mixed-gas adsorption equilibria on heterogeneous solid surfaces. In *Equilibria and Dynamics of Gas Adsorption on Heterogeneous Solid Surfaces*; Rudzinski, W., Steele, W.A., Zgrablich, G., Eds.; Elsevier: Amsterdam, The Netherlands, 1997; pp. 1–104.

49. Dodge, Y. *The Concise Encyclopedia of Statistics*; Springer: Berlin/Heidelberg, Germany, 2008; p. 616.

50. Ishikawa, K.; Tanaka, M.; Suzuki, T.; Sekine, A.; Kawasaki, T.; Soai, K.; Shiro, M.; Lahav, M.; Asahi, T. Absolute chirality of the c-polymorph of glycine: Correlation of the absolute structure with the optical rotation. *Chem. Commun.* **2012**, *48*, 6031–6033. [CrossRef] [PubMed]

51. Schlueter, A.W.; Jacobson, R.A.; Rundle, R.E. A Redetermination of the Crystal Structure of $CsCuCl_3$. *Inorg. Chem.* **1966**, *5*, 277–280. [CrossRef]

52. Wang, L.; Kong, H.; Song, X.; Liu, X.; Wang, H. Chiral supramolecular self-assembly of rubrene. *Phys. Chem. Chem. Phys.* **2010**, *12*, 14637–14832. [CrossRef]